Dissipative light scattering by a trapped atom approaching electromagnetically-induced-transparency conditions

Maryam Roghani,[*] Heinz-Peter Breuer,[†] and Hanspeter Helm[‡]
Institute of Physics, Albert-Ludwigs University, Hermann-Herder Strasse 3, D-79104 Freiburg, Germany
(Received 16 September 2009; revised manuscript received 15 January 2010; published 22 March 2010)

We study the time dependence of the spectrum of inelastically scattered radiation from a trapped atom. The atom is illuminated by two lasers tuned to the electromagnetically induced transparency (EIT) of the free atom. For counterpropagating laser beams, rapid removal of vibrational energy is observed as the atom approaches near-EIT conditions. We show that the imbalance in the sidebands of the scattered radiation spectrum explains quantitatively the cooling of the center-of-mass motion of the trapped atom. We also examine parameters critical for EIT cooling in situations far from the Lamb-Dicke limit.

DOI: 10.1103/PhysRevA.81.033418 PACS number(s): 37.10.De, 42.50.Gy, 42.50.Tx

I. INTRODUCTION

Laser cooling of a trapped three-level ion, driven by two counterpropagating laser beams, was first analyzed by Lindberg and Javanainen [1] in 1986. The authors obtained steady-state solutions by expanding the corresponding quantum master equation to the second order in the Lamb-Dicke parameter. This dimensionless parameter describes the ratio of the amplitude of the trapped-atom motion and the wavelength of the driving laser. When expressed in terms of recoil energy over trap vibrational energy, the squared Lamb-Dicke parameter reads

$$\eta^2 = \frac{\hbar k^2}{2M\omega}, \tag{1}$$

with M being the mass of the trapped atom, ω being the harmonic oscillator (HO) trap frequency, and k being the characteristic wave number of the laser light. Fixing one of the lasers at a frequency of less than the resonance transition $|1\rangle \rightarrow |3\rangle$ (see the transitions in Fig. 1), the authors studied the competition between heating and cooling in the limit of low laser intensities. They found the cooling was most efficient if the second laser is also red-detuned from its resonance transition $|2\rangle \rightarrow |3\rangle$ by an amount equal to the trap frequency. When the trap frequency is larger than the excited-state decay rate, this cooling mechanism may be termed *sideband cooling*. Lindberg and Javanainen also showed that in the limit of very large and equal detunings, reversible two-photon transitions $|1, n\rangle \leftrightarrow |2, n \pm 1\rangle$ can be tailored to cool atomic motion if the laser intensities are chosen to be unequal [1]. For this case, the authors predicted a limiting temperature of the order of the two-photon line width, Γ_{12}, which may be made extremely small.

In 2000, Morigi *et al.* [2] refined this analysis (in the Lamb-Dicke limit) further by optimizing the effect of electromagnetically-induced-transparency (EIT) resonance for the cooling cycle. For large blue detuning and two-photon resonance $\omega_{L1} - \omega_{L2} = \omega_{21}$,[1] transient coherent population trapping can occur, and the vibrational motion can be efficiently cooled to the ground state of the trapping potential. This situation is optimized if one of the lasers (from here on called the *pump laser*) is intense and the ac-Stark shift induced by the pump laser is chosen to be of the order of the vibrational trap frequency. As the carrier transition is suppressed by EIT, the asymmetric EIT line shape may induce a strong imbalance between cooling and heating transitions. The imbalance favors cooling when the detuning is chosen positive,

$$\begin{aligned} \Delta_1 &= \omega_{L1} - \omega_{31} > 0, \\ \Delta_2 &= \omega_{L2} - \omega_{32} > 0, \end{aligned} \tag{2}$$

and equal, $\Delta_1 = \Delta_2$.

The EIT cooling scheme has been successfully realized for trapped ions [3], and it is tempting to contemplate a transfer of this scheme to cooling and state manipulation of neutral atoms. EIT cooling of trapped neutral atoms is prone to be superior to velocity-selective coherent population trapping (VSCPT) of free atoms [4], which lacks the ability of spatial confinement. However, a caveat for application with trapped neutral atoms is that the Lamb-Dicke parameters that can be realized experimentally are not typically small since neutral-atom-trap frequencies usually fall below ≈50 kHz and recoil energies are in the range of a few kilohertz. It is for this reason that we have recently extended Morigi's analysis [5] to situations not restricted to the Lamb-Dicke limit [6]. When η is not very small, many sidebands are active, as is apparent from Fig. 2. Nevertheless, we showed that even at elevated values of the Lamb-Dicke parameter, fast cooling rates can be achieved, albeit to mean vibrational values greater than those predicted in the Lamb-Dicke limit [6].

In the current work, we aim to analyze the temporal development of EIT cooling and identify the origin of dissipative terms in the interaction of the trapped atom with light. To this end, we have performed extensive numerical simulations of the quantum master equation, which models the dissipative dynamics of the full-density matrix, describing both the external and the internal degrees of freedom of the atom.

[*]maryam.roghani@physik.uni-freiburg.de
[†]breuer@physik.uni-freiburg.de
[‡]helm@uni-freiburg.de

[1]The electronic energy differences are given in terms of the electronic state energies ω_i by the relationship $\omega_{ij} = \omega_i - \omega_j$.

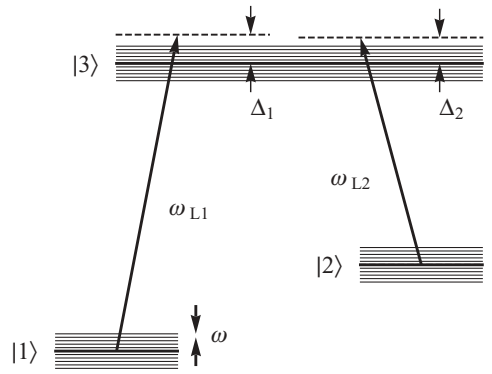

FIG. 1. Trapped three-level atom in the presence of two counterpropagating lasers at the frequencies ω_{L1} and ω_{L2}. The trap frequency is ω.

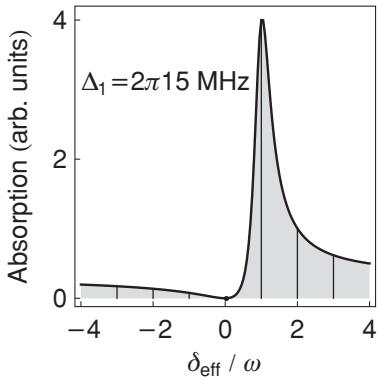

FIG. 3. Close up of EIT-resonance line shape in the Lamb-Dicke limit for absorption of laser 2 at the parameters used in the simulations. Frequencies, given in units of 2π MHz, are $g_1 = 1.3$, $g_2 = 0.3$, $\Delta = 15$, and $\Gamma = 6$. The effective detuning of laser 2 from the EIT resonance is defined as $\delta_{\text{eff}} = \Delta_2 - \Delta_1$.

We show that spontaneous emission of a trapped atom always gives rise to vibrational heating. The vibrational heating rate in spontaneous emission scales as η^2 and, hence, increases the farther away one is from the Lamb-Dicke limit. However, the spontaneous heating can be outweighed by radiative cooling, which occurs as a result of an imbalance in the radiation field formed when the trapped atom scatters laser radiation. The spectral imbalance around the two Rayleigh lines is a consequence of nonlinear Raman scattering and it is the fundamental mechanism for EIT cooling, as we demonstrate later. When the Lamb-Dicke parameter is not zero, *unbalanced vibrational sidebands* appear in the scattered laser fields. These arise from nonlinear coherences among vibronic states. The sidebands are unbalanced in favor of cooling in case the two EIT lasers are blue-detuned from resonance. We demonstrate that the major part of the energy carried away through inelastic scattering of laser radiation leads to a vibrational cooling of the atomic motion, whereas only a small part of this energy contributes to the change of the internal atomic energy and of the atom-laser interaction energy.

The article is organized as follows. After describing our numerical approach to treating the trapped atom in the presence of the two running wave laser fields, we discuss typical results for the temporal development of vibrational cooling. This is followed by an analysis of the force and energy-loss terms active in this model and by a study of the temporal development of the radiation fields, which are scattered from the incoming laser fields by the trapped atom.

II. THEORETICAL MODEL

A. Time evolution of internal and external degrees of freedom of the atom

We study a Λ-shaped, three-level atom trapped in a harmonic potential under the action of two counterpropagating laser beams. The laser conditions are adjusted to promote EIT cooling [6]; that is, both lasers are blue-detuned but are on two-photon resonance, $\omega_{L1} - \omega_{L2} = \omega_{21}$. The ac-Stark shift induced by the strong laser (in the following termed *laser 1*, with Rabi frequency g_1) is chosen to be of the order of the vibrational trap frequency,

$$\omega \approx \frac{1}{2}\left(\Delta_1 + \sqrt{g_1^2 + \Delta_1^2}\right). \tag{3}$$

A consequence of this setting is apparent from Fig. 3, which gives the absorption line profile for laser 2 in the Lamb-Dicke limit.

The horizontal scale is the detuning of laser 2 from EIT resonance, $\delta_{\text{eff}} = \Delta_2 - \Delta_1$. Under condition (3), the first sideband for cooling, at $\delta_{\text{eff}}/\omega = +1$, is optimized over that

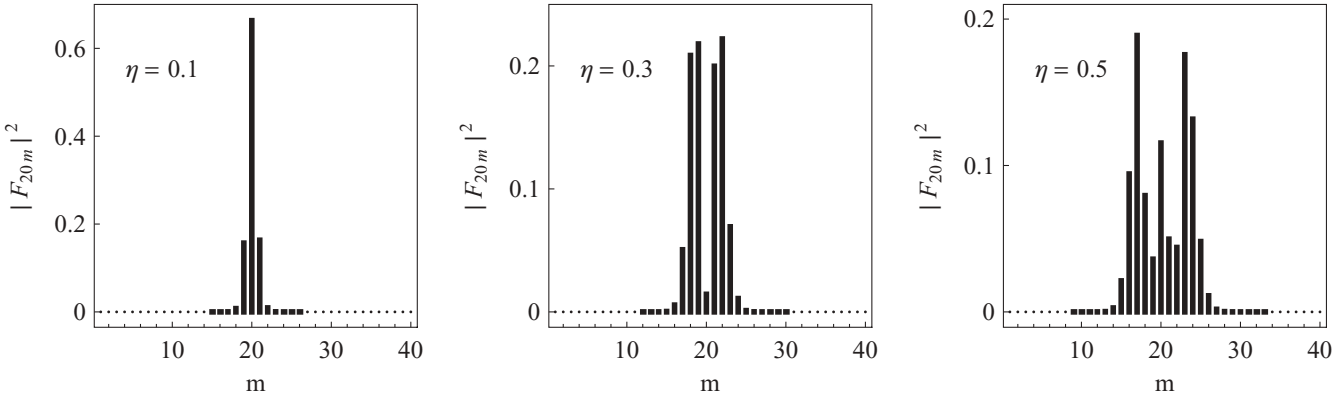

FIG. 2. Strength of sideband transitions from $n = 20$ for three values of η.

for heating, at $\delta_{\rm eff}/\omega = -1$. As $\omega_{L1} - \omega_{L2} = \omega_{21}$, the atom precisely satisfies EIT conditions for $\eta = 0$, and it will nearly do so [6] at small values of the Lamb-Dicke parameter. In order to describe the time evolution of the trapped-atom case, away from the Lamb-Dicke limit, correlations and entanglement between internal and external degrees of freedom have to be accounted for. These are important ingredients in the dynamics of cooling and in the approach to the near-EIT condition that is reached in the stationary state. The time evolution of the three-level, Λ-shaped atom trapped in a one-dimensional HO potential is examined by solving the quantum master equation

$$\frac{\partial \hat{\tilde{\rho}}}{\partial t} = \hat{\mathcal{L}}\hat{\tilde{\rho}} \equiv -\frac{\rm i}{\hbar}[\hat{\mathcal{H}}, \hat{\tilde{\rho}}] + \hat{\mathcal{L}}_0\hat{\tilde{\rho}}. \tag{4}$$

The density matrix $\hat{\tilde{\rho}}$ describes the state of the composite system consisting of both the electronic and the vibrational degrees of freedom of the atom. Denoting the electronic states by $|i\rangle$, $i = 1, 2, 3$ and the vibrational states (Fock states) by $|n\rangle$, $n = 0, 1, 2, \ldots$, the density matrix can be represented in terms of the product basis $|i, n\rangle = |i\rangle \otimes |n\rangle$ as

$$\hat{\tilde{\rho}} = \sum_{i,j,n,m} \tilde{\rho}_{injm} |i, n\rangle\langle j, m|. \tag{5}$$

The Hamiltonian $\hat{\mathcal{H}}$ describes the motion of the atomic center of mass (cm), the internal electronic dynamics (el), and the interaction of the atom with the two laser beams (int),

$$\hat{\mathcal{H}} = \hat{\mathcal{H}}_{\rm cm} + \hat{\mathcal{H}}_{\rm el} + \hat{\mathcal{H}}_{\rm int}. \tag{6}$$

The Hamiltonian for the HO with trap frequency ω can be written as

$$\begin{aligned}\hat{\mathcal{H}}_{\rm cm} &= \sum_n \hbar\omega n |n\rangle\langle n| + \frac{\hbar\omega}{2} = \frac{p^2}{2M} + \frac{1}{2}M\omega^2 x^2 \\ &= \frac{\hbar\omega}{2}(\mathcal{P}^2 + \mathcal{Q}^2),\end{aligned} \tag{7}$$

where we have used the HO length $a_0 = \sqrt{\hbar/(M\omega)}$ to define dimensionless position and momentum operators through $\mathcal{Q} = x/a_0$ and $\mathcal{P} = pa_0/\hbar$. By transforming to an interaction picture and employing the rotating wave approximation [7], one finds the electronic configuration Hamiltonian [8],

$$\hat{\mathcal{H}}_{\rm el} = +\hbar\Delta_1|1\rangle\langle 1| + \hbar\Delta_2|2\rangle\langle 2|, \tag{8}$$

and the Hamiltonian describing the interaction with the laser beams,

$$\hat{\mathcal{H}}_{\rm int} = \frac{\hbar}{2}(g_1^* e^{-{\rm i}\vec{k}_1\cdot\vec{x}}|1\rangle\langle 3| + g_2^* e^{-{\rm i}\vec{k}_2\cdot\vec{x}}|2\rangle\langle 3| + {\rm H.c.}). \tag{9}$$

We assume that $|\omega_{21}| \ll \omega_{31} \approx \omega_{32}$, but at the same time $\omega_{31} - \omega_{32} \gg \Gamma$, where Γ is the natural width of the excited state. In this case, we are allowed to postulate that laser 1 only interacts with the $|1\rangle \leftrightarrow |3\rangle$ transition whereas laser 2 acts on the $|2\rangle \leftrightarrow |3\rangle$ transition. By the same argument, we may set $\eta_1 \approx \eta_2 = \eta$, and we abbreviate the Franck-Condon factors by

$$\langle n|e^{\pm{\rm i}\vec{k}_q\cdot\vec{x}}|m\rangle = F_{nm}^{(\pm\eta)}. \tag{10}$$

The Franck-Condon factors control the strength of sideband transitions. In the Lamb-Dicke limit ($\eta \to 0$), we have $F_{nn}^{(\eta)} \approx 1$ and $F_{nn+1}^{(\eta)} = F_{n+1n}^{(\eta)} = {\rm i}\sqrt{n+1}\eta(1 + O[\eta^2])$. The explicit form of these factors is given in Eq. (B9) of Ref. [6].

Relaxation due to spontaneous emission leads to a loss of population in the electronically excited vibrational states $|3, n\rangle$ and gain of population by the ground-state levels $|1, n'\rangle$ and $|2, n'\rangle$. The Frank-Condon factors control how the population is distributed over the vibrational manifold. Spontaneous emission also leads to a loss of coherence between electronic and vibrational levels. These effects of spontaneous emissions are described by the last term of the master equation (4), which is explicitly given by [9]:

$$\hat{\mathcal{L}}_0\hat{\tilde{\rho}} = \sum_{j=1,2}\sum_{q=\pm}\frac{\Gamma_j}{2}\left[\sigma_{jq}^- \hat{\tilde{\rho}}\sigma_{jq}^+ - \frac{1}{2}\{\sigma_{jq}^+\sigma_{jq}^-, \hat{\tilde{\rho}}\}\right]. \tag{11}$$

We have written this superoperator in the standard Lindblad form (see, e.g., [10]) involving the Lindblad operators

$$\sigma_{jq}^- = |j\rangle\langle 3|e^{{\rm i}qk_j x} \quad \text{and} \quad \sigma_{jq}^+ = |3\rangle\langle j|e^{-{\rm i}qk_j x}, \tag{12}$$

where $q = \cos\theta$ describes the angle of $\vec{k}$ with respect to the trap axis. For technical simplicity, we assume that the direction of $\vec{k}$ in spontaneous emission is only parallel or antiparallel to the HO axis. Hence, for example, the operator σ_{jq}^- describes the spontaneous transitions $|3\rangle \to |j = 1, 2\rangle$ corresponding to the emission of a photon parallel ($q = +1$) or antiparallel ($q = -1$) to the oscillator axis. The second term in Eq. (11) describes the loss of coherence due to spontaneous emission, providing terms of the form ($j = 1, 2, 3$),

$$\frac{\partial}{\partial t}\tilde{\rho}_{3njm} = -\frac{\Gamma}{2}\tilde{\rho}_{3njm}, \tag{13}$$

and of the form ($i = 1, 2, 3$),

$$\frac{\partial}{\partial t}\tilde{\rho}_{in3m} = -\frac{\Gamma}{2}\tilde{\rho}_{in3m}. \tag{14}$$

For $i = j = 3$ and $n = m$, Eqs. (13) and (14) describe the loss of excited-state population. The first term of Eq. (11) can be expressed in terms of Franck-Condon factors. With $|\omega_{21}| \ll \omega_{31} \approx \omega_{32}$, a single value of η suffices for all spontaneous emission events. This gives us, for $j = 1, 2$,

$$\frac{\partial}{\partial t}\tilde{\rho}_{jnjm} = \frac{\Gamma}{4}\sum_{o,p}\tilde{\rho}_{3o3p}\left[F_{np}^{(\eta)}F_{om}^{(-\eta)} + F_{np}^{(-\eta)}F_{om}^{(\eta)}\right]. \tag{15}$$

where the summation over o and p covers all vibrational levels of the HO. Here, we made the assumption of even branching ($\Gamma_1 = \Gamma_2$) of spontaneous events between the electronic ground-state levels $|1\rangle$ and $|2\rangle$. The contributions from Eq. (15) fall into two classes: One type ($n = m$) describes the gain of population by the electronic ground states, and the second type ($n \neq m$) describes transfer of spatial coherence in the event of spontaneous emission.

B. Time evolution of the scattered radiation field

In addition to the classical laser fields introduced in Eq. (9), we now also consider the quantum radiation field formed as a consequence of scattering laser radiation. The Hamiltonian for this field (which initially is in the vacuum state) and for the

interaction of the atom with this field is

$$\begin{aligned}\hat{\mathcal{H}}_S &= \hat{\mathcal{H}}_R + \hat{\mathcal{H}}_{RA} \\ &= \sum_{\vec{k},\lambda} \hbar\omega_{\vec{k},\lambda} \hat{b}^\dagger_{\vec{k},\lambda} \hat{b}_{\vec{k},\lambda} + \sum_{j=1,2} \sum_{q=\pm} \frac{\hbar}{2} (\sigma^-_{jq} \hat{b}^\dagger_{\vec{k},\lambda} g^*_{\vec{k},\lambda} \\ &\quad + \sigma^+_{jq} \hat{b}_{\vec{k},\lambda} g_{\vec{k},\lambda}), \end{aligned} \tag{16}$$

where $\hat{b}_{\vec{k},\lambda}, \hat{b}^\dagger_{\vec{k},\lambda}$ are the annihilation and creation operators for the field quanta and the frequencies $g_{\vec{k},\lambda} = -\frac{\vec{d}\cdot\vec{E}^0_{\vec{k},\lambda}}{\hbar}$ are the products of the electric dipole moment of the atom, $\vec{d}$, and the respective amplitude of the quantum radiation field $\vec{E}$

$$\vec{E}(\vec{x}) = \mathrm{i} \sum_{\vec{k},\lambda} \vec{E}^0_{\vec{k},\lambda} (\hat{b}_{\vec{k},\lambda} \mathrm{e}^{\mathrm{i}\vec{k}\cdot\vec{x}} - \hat{b}^\dagger_{\vec{k},\lambda} \mathrm{e}^{-\mathrm{i}\vec{k}\cdot\vec{x}}). \tag{17}$$

The summation over $\vec{k}$ and λ refers to the summation over the wave-vector components and polarization directions. For the ease of reading, we define $k = (\vec{k}, \lambda)$ in the following. We are interested in the time evolution of the scattered field quanta. To this aim, the Heisenberg equation leads us to

$$\frac{d\hat{b}_k(t)}{dt} = \frac{\mathrm{i}}{\hbar} [\hat{\mathcal{H}}_S, \hat{b}_k(t)]. \tag{18}$$

Applying the relation $[\hat{b}_k, \hat{b}^\dagger_k] = 1$, we get

$$\frac{d\hat{b}_k(t)}{dt} = -\mathrm{i}\omega_{\vec{k}} \hat{b}_k(t) - \frac{\mathrm{i}}{2} \sum_{jq} g^*_k \sigma^-_{jq}(t), \tag{19}$$

with the solution

$$\begin{aligned}\hat{b}_k(t) &= \hat{b}_k(t=0)\mathrm{e}^{-\mathrm{i}\omega_k t} \\ &\quad - \frac{\mathrm{i}}{2} g^*_k \sum_{jq} \int_0^t d\tau \sigma^-_{jq}(t-\tau) \mathrm{e}^{-\mathrm{i}\omega_k(t-\tau)}. \end{aligned} \tag{20}$$

The time when our cooling experiment begins is taken as $t = 0$. Hence, the first term in Eq. (20) gives us the initial field having evolved freely over the time period t, and the second term gives us the field created by the atomic dipole during this time period. The power carried away by the field of scattered radiation field at time t can therefore be expressed as

$$\begin{aligned}\mathcal{P}(t) &= \frac{d}{dt} \sum_k \hbar\omega_k \langle \hat{b}^\dagger_k(t) \hat{b}_k(t) \rangle \\ &= \sum_k \hbar\omega_k \left\langle \frac{d\hat{b}^\dagger_k(t)}{dt} \hat{b}_k(t) \right\rangle + \mathrm{H.C.} \\ &= 2\mathrm{Re} \sum_k \hbar\omega_k \left\langle \frac{d\hat{b}^\dagger{}_k(t)}{dt} \hat{b}_k(t) \right\rangle. \end{aligned} \tag{21}$$

Substituting Eq. (20) and the Hermitian conjugate of Eq. (19) in Eq. (21) gives us

$$\begin{aligned}\mathcal{P}(t) = 2\mathrm{Re} \sum_k \hbar\omega_k \Bigg[&\mathrm{i}\omega_k \mathrm{e}^{-\mathrm{i}\omega_k t} \langle \hat{b}^\dagger_k(t) \hat{b}_k(t=0) \rangle \\ &+ \frac{\mathrm{i}}{2} g_k \mathrm{e}^{-\mathrm{i}\omega_k t} \sum_{jq} \langle \sigma^+_{jq}(t) \hat{b}_k(t=0) \rangle \\ &- \frac{1}{2} g^*_k \omega_k \sum_{jq} \int_0^t d\tau \langle \hat{b}^\dagger_k(t) \sigma^-_{jq}(t-\tau) \rangle \mathrm{e}^{-\mathrm{i}\omega_k(t-\tau)} \\ &+ \frac{1}{4} |g_k|^2 \sum_{jq} \int_0^t d\tau \langle \sigma^+_{jq}(t) \sigma^-_{jq}(t-\tau) \rangle \mathrm{e}^{-\mathrm{i}\omega_k(t-\tau)} \Bigg]. \end{aligned} \tag{22}$$

The first three terms on the right-hand side of Eq. (22) may be neglected within the Markovian approximation. We now use the substitution $\sum_k \frac{|g_k|^2}{2} \to \int_0^\infty d\omega_k \int d\Omega_k D(\omega_k)$ [11], while $g_k = \sqrt{\omega_k/(2\hbar\epsilon_0 V)} \vec{d} \cdot \hat{\mathrm{e}}_k$, where $\vec{d}$ is the atomic dipole momentum and $\hat{\mathrm{e}}_k$ is the field polarization vector. $D(\omega_k) = \frac{1}{2} \frac{(2V)}{(2\pi)^3} |g_k|^2$, and $\int d\Omega_k = \int_0^{2\pi} d\phi \int_0^\pi d\theta \sin\theta$, θ being the angle between the dipole moment and the wave vector. The scattered laser photons are all near the respective laser frequency; therefore, we may write for the emission rate $D(\omega_k) \approx D(\omega_L) = \Gamma_j / 4\pi^2$ and obtain, when summing over the contribution to scattering from both lasers fields,

$$\begin{aligned}\mathcal{P}(t) = \sum_{jq} \frac{\Gamma_j}{4\pi^2} \int_0^\infty d\omega_k \int d\Omega_k \hbar\omega_k \, \mathrm{Re} \\ \times \int_0^t d\tau \langle \sigma^+_{jq}(t) \sigma^-_{jq}(t-\tau) \rangle \mathrm{e}^{-\mathrm{i}\omega_k \tau}. \end{aligned} \tag{23}$$

Substituting $\omega' = \omega_k - \omega_L$ and defining

$$\mathcal{S}^q_j(\omega', t) = \mathrm{Re} \int_0^t d\tau \langle \sigma^+_{jq}(t) \sigma^-_{jq}(t-\tau) \rangle \mathrm{e}^{-\mathrm{i}\omega'\tau} \tag{24}$$

gives us

$$\mathcal{P}(t) = \sum_{jq} \frac{\Gamma_j}{4\pi^2} \int_{-\omega_L}^\infty d\omega' \int d\Omega_k \hbar(\omega' + \omega_L) \mathcal{S}^q_j(\omega', t). \tag{25}$$

Photons scattered at the frequency $\omega_k = \omega_L$ do not contribute to a change of the energy of the trapped atom. Therefore, we may define the cooling/heating rate of the trapped atom system that arises from inelastic scattering of laser radiation as

$$\mathcal{R}(t) = \sum_{jq} \frac{\Gamma_j}{4\pi^2} \int d\Omega_k \int_{-\infty}^\infty d\omega' \hbar\omega' \mathcal{S}^q_j(\omega', t). \tag{26}$$

Here we have substituted the lower integration limit $-\omega_L$ by $-\infty$ as $\omega' \ll \omega_L$. Again for technical simplicity, we consider the case that half of the scattered photons propagate parallel and half antiparallel to the trap axis; hence,

$$\mathcal{R}(t) = \sum_j \frac{\Gamma_j}{2\pi} \int_{-\infty}^{+\infty} d\omega' \hbar\omega' \left[\mathcal{S}^{+1}_j(\omega', t) + \mathcal{S}^{-1}_j(\omega', t) \right]. \tag{27}$$

The weighting of the spectrum $\mathcal{S}$ by $\hbar\omega'$ gives us a signed measure of the imbalance in energy between the laser photons and the scattered photons. If the scattered field is symmetric around ω_L, on average no net change of energy occurs. On the other hand, if the scattered field has unbalanced sidebands, then cooling or heating of the vibrational state of the trapped atom may occur, with $\mathcal{R}(t)$ being positive in case of cooling.

III. NUMERICAL SOLUTION

To evaluate the time dependence of density matrix of the entangled system under conditions not restricted to the

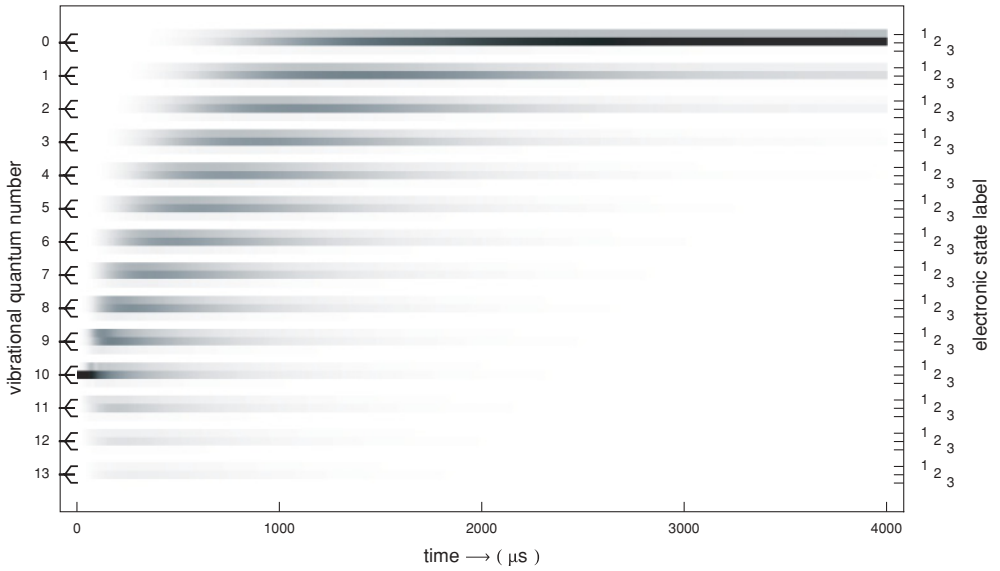

FIG. 4. Map of populations in the three electronic states for cooling from the initial Fock state ($n = 10$) in state $|2\rangle$.

Lamb-Dicke limit, we opted for a numerical solution of the master equation. The numerical approach is well suited to develop expressions for the terms that describe the time dependence of transfer of momentum and vibrational energy as they are active in cooling. This permits us to examine the dynamics responsible for removal of vibrational energy as well as to estimate realistic cooling times and to examine parameters that are critical to be met in an experiment. Most important, it permits us to examine the temporal evolution of the spectrum of scattered radiation field.

We solve Eq. (4) numerically for a one-dimensional trap for the three electronic levels shown in Fig. 1. We consider the case of antiparallel laser beams where $\vec{k}_1$ propagates parallel to $\vec{x}$ while $\vec{k}_2$ propagates antiparallel to $\vec{x}$. We assume the vibrational trap spacing ω to be identical in all three electronic states, and we limit the number of vibrational levels included in each electronic state to $m_{\max}$.

Figure 4 shows a typical result for the development of populations during the cooling process. The laser intensities are ramped[2] to full power over the first 100 μs and are then held constant from that time onward. The parameters are $m_{\max} = 21$ and $\eta = 0.1$, and the frequencies (given in units of 2π MHz) are $\omega = 0.03$, $g_1 = 1.3$, $g_2 = 0.3$, $\Delta = 15$, and $\Gamma = 6$. These optimized parameters lead to rapid cooling. We note from Fig. 4 that the population is rapidly transferred from the initial vibrational level $n = 10$ into the ground vibrational level. A very small amount of population initially migrates to higher vibrational levels but is rapidly cooled down as well.[3] The excited electronic state is hardly ever populated (we always have $\sum_n \rho_{3n3n} < 10^{-4}$). The electronic-state distribution after 3 ms closely approaches the EIT situation for free atoms, with the electronic population ratio being $\sum_n \rho_{1n1n} / \sum_n \rho_{2n2n} \approx (g_2/g_1)^2$. After 3 ms, $\langle n \rangle$ is very close to the stationary-state result of Eq. (4), which yields $\langle n \rangle_{\rm st} = 0.0144$. For comparison, the stationary-state solution in the Lamb-Dicke limit [2] predicts $\langle n \rangle_{\rm st} = 0.008$.

In order to illuminate the mechanism responsible for removal of vibrational energy from the trapped atom, we now examine the temporal development of the individual force and energy exchange terms, as well as the temporal development of the field of radiation scattered by the trapped atom.

A. Analysis of force terms

The expectation value of the momentum operator may be compared to the result of the equation of motion for the mean momentum, which follows from the master equation (4),

$$\frac{d}{dt}\langle \mathcal{P} \rangle = \frac{\mathrm{i}}{\hbar}\langle [H_{\rm cm}, \mathcal{P}] \rangle + \frac{\mathrm{i}}{\hbar}\langle [H_{\rm int}, \mathcal{P}] \rangle + \mathrm{tr}\{\mathcal{P}\hat{\mathcal{L}}_0\hat{\tilde{\rho}}\} \equiv \langle F_{\rm HO} \rangle + \langle F_{\rm int} \rangle + \langle F_{\rm sp} \rangle. \tag{28}$$

Here,

$$\langle F_{\rm HO} \rangle = -\omega \langle \mathcal{Q} \rangle \tag{29}$$

is the harmonic oscillator force, and

$$\langle F_{\rm int} \rangle = \frac{\mathrm{i}\hbar k}{2} \sum_{n,p} \left[(g_1^* \rho_{3n1p} + g_2 \rho_{2n3p}) F_{pn}^{(-\eta)} - (g_1 \rho_{1n3p} + g_2^* \rho_{3n2p}) F_{pn}^{(+\eta)} \right] \tag{30}$$

represents the laser interaction force due to photon recoil in stimulated absorption and emission. The signs of the terms in Eq. (30) are dictated by the directions of laser propagation. In our case, laser 1 propagates into the positive x direction, while laser 2 propagates into the negative x direction. We may separate the force terms from lasers 1 and 2 by writing $\langle F_{\rm int} \rangle = \langle F_{\rm int}^1 \rangle + \langle F_{\rm int}^2 \rangle$. Finally, the average force due to spontaneous emission processes, $\langle F_{\rm sp} \rangle$, can easily be seen

[2]The laser intensities for $0 < t < t_{\rm on}$ are turned on according to $I(t) = I_0 \sin^2 [\pi t/(2t_{\rm on})]$, with $t_{\rm on}$ being the turn-on time.

[3]The results shown are found to be independent of the upper limit $m_{\max}$ as long as $m_{\max} \gtrsim 1.5 n_{\rm init}$ for $\eta = 0.1$. For larger η values, $m_{\max}$ has to be chosen progressively higher.

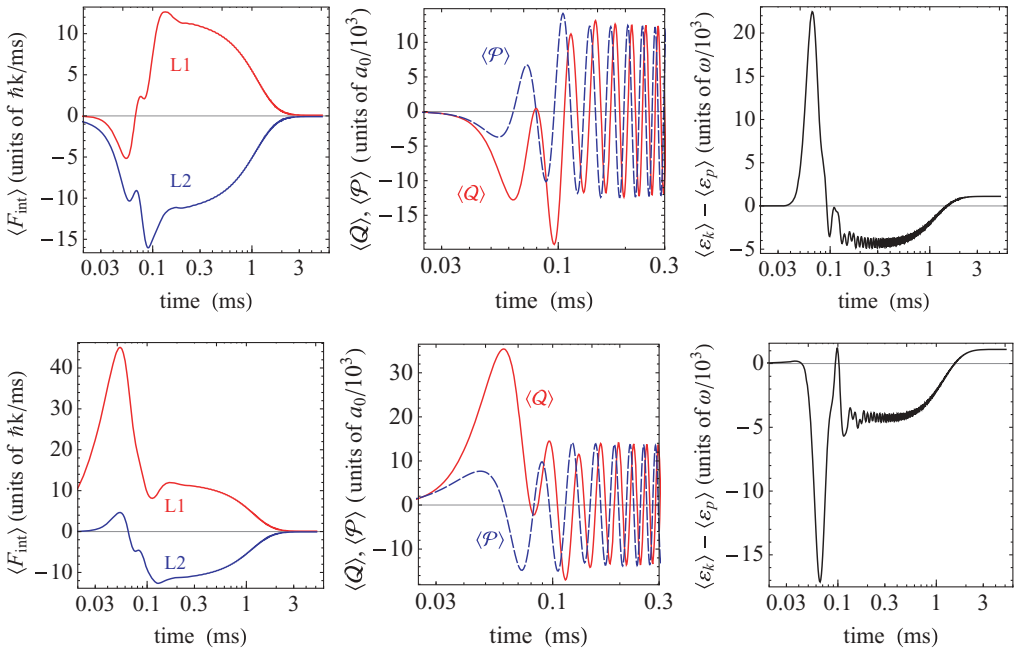

FIG. 5. (Color online) Interaction force terms from laser L1 (upper line) and laser L2 (lower line) are compared to the response in mean position $\langle\mathcal{Q}\rangle$ (full line) and momentum $\langle\mathcal{P}\rangle$ (dashed line). Also shown is the difference between mean kinetic and potential energy. The top row gives the result when the initial Fock state ($n = 10$) is in the electronic state $|2\rangle$. In the bottom row, the system is initially in the electronic state $|1\rangle$.

to vanish identically. The master equation yields

$$\begin{aligned}\langle F_{\rm sp}\rangle &= {\rm tr}\{\mathcal{P}\hat{\mathcal{L}}_0\hat{\tilde{\rho}}\}\\ &= \sum_j \frac{\Gamma_j}{2}{\rm tr}\{(e^{-{\rm i}k_jx}\mathcal{P}e^{{\rm i}k_jx} - \mathcal{P})|3\rangle\langle 3|\hat{\tilde{\rho}}\\ &\quad + (e^{{\rm i}k_jx}\mathcal{P}e^{-{\rm i}k_jx} - \mathcal{P})|3\rangle\langle 3|\hat{\tilde{\rho}}\}. \end{aligned} \tag{31}$$

Since $e^{-{\rm i}k_jx}\mathcal{P}e^{{\rm i}k_jx} - \mathcal{P} = \hbar k_j$, we find

$$\langle F_{\rm sp}\rangle = \sum_j \frac{\Gamma_j\hbar k_j}{2}{\rm tr}\{|3\rangle\langle 3|\hat{\tilde{\rho}} - |3\rangle\langle 3|\hat{\tilde{\rho}}\} = 0. \tag{32}$$

As expected, the momentum kicks induced by spontaneous emission processes on average exactly cancel each other. There is thus no dissipative force term in our model that results from spontaneous emission. This is also borne out by the numerical solution. We show in Fig. 5 the individual force terms from Eqs. (29) and (30). Their numerical sum precisely matches the time derivative of the mean atomic momentum, the left-hand side of Eq. (28).

It is interesting to discuss the temporal evolution of the momentum transfer for two different initial conditions. In Fig. 5 (top row), the atom is initially in vibrational level $n = 10$ of electronic state $|2\rangle$; hence, laser 2 must be active initially. Absorption of photons from laser 2 pushes the atom to negative $\langle\mathcal{Q}\rangle$ values, being aided by stimulated emission into laser beam 1, a process that also recoils the atom in the direction of negative $\langle\mathcal{Q}\rangle$. In the following, the population transfer to state $|1\rangle$ reverses the situation, and after an equilibration phase lasting for about 200 μs, the atomic center of mass begins a harmonic oscillation with trap frequency ω. This motion is damped exponentially. In Fig. 5 (bottom row), the atom is initially in electronic state $|1\rangle$. We see that in this case laser 1 is active initially. Absorption of photons from laser 1 pushes the atom to positive $\langle\mathcal{Q}\rangle$ values, being aided by stimulated emission into laser beam 2, which also recoils the atom in the direction of positive $\langle\mathcal{Q}\rangle$. Both conditions eventually reach the same long-time limit in our numerical simulation, as it should be the case.

If we consider the center-of-mass energy of the atom $\langle\mathcal{E}_{\rm cm}\rangle = \langle\mathcal{E}_{\rm k}\rangle + \langle\mathcal{E}_{\rm p}\rangle = \frac{1}{2}\big(\langle\mathcal{Q}^2\rangle + \langle\mathcal{P}^2\rangle\big)$, it follows precisely the temporal development of $\langle n\rangle$. On the other hand, the difference between kinetic and potential energy, $\langle\mathcal{E}_{\rm k}\rangle - \langle\mathcal{E}_{\rm p}\rangle$, reflects the dynamics of the atomic motion. The results for the difference [see Figs. 5(c) and (f)] are consistent with the time-dependent forces acting on the atom. A wave packet develops from the initial Fock state, the excess of motional energy diminishing during the equilibration phase. After about 200 μs, a kind of regular motion develops, as is reflected by the periodic oscillation of $\langle\mathcal{E}_{\rm k}\rangle - \langle\mathcal{E}_{\rm p}\rangle$ at the HO frequency. This motion is damped in an exponential fashion to an eventually slightly positive value, which scales $\propto \eta^2$. This long-term value for the difference is identical to that obtained in the stationary-state solution of Eq. (4). The explicit expression for $\langle\mathcal{E}_{\rm k}\rangle - \langle\mathcal{E}_{\rm p}\rangle$,

$$\begin{aligned}\langle\mathcal{E}_{\rm k}\rangle - \langle\mathcal{E}_{\rm p}\rangle = -\frac{1}{2}\sum_{i,n}[&\sqrt{(n+1)(n+2)}\tilde{\rho}_{inim}\delta(m,n+2)\\ &+\sqrt{n(n-1)}\tilde{\rho}_{inim}\delta(m,n-2)],\end{aligned} \tag{33}$$

shows that this difference reflects the presence of vibrational coherences $\tilde{\rho}_{ini(n\pm2)}$ in the stationary state. These coherences reflect the residual pumping in the stationary state; for a pure dark state, they tend to zero.

B. Vibrational energy loss

In the Heisenberg picture, we have for the time evolution of the vibrational energy of the atom

$$\frac{d}{dt}\langle\hat{\mathcal{H}}_{\rm cm}\rangle = \frac{\rm i}{\hbar}\langle[\hat{\mathcal{H}}_{\rm int},\hat{\mathcal{H}}_{\rm cm}]\rangle + {\rm tr}\{\hat{\mathcal{H}}_{\rm cm}\hat{\mathcal{L}}_0\hat{\tilde{\rho}}\} = \langle\dot{\mathcal{E}}_{\rm int}\rangle\hbar\omega + \langle\dot{\mathcal{E}}_{\rm sp}\rangle\hbar\omega, \tag{34}$$

which we separate into rates of vibrational energy transfer resulting from interaction with the two lasers, $\langle\dot{\mathcal{E}}_{\rm int}\rangle$, and from spontaneous emission, $\langle\dot{\mathcal{E}}_{\rm sp}\rangle$. The term containing the commutator delivers expressions involving the vibrational number operator $\hat{\mathcal{N}}$. It can be analyzed by sandwiching the identity operator $\sum_m |m\rangle\langle m| = 1$,

$$\sum_{m,n}|m\rangle\langle m|{\rm e}^{{\rm i}kx}\hat{\mathcal{N}}|n\rangle\langle n| = \sum_{n,m} n F^{(+\eta)}_{nm}|m\rangle\langle n|. \tag{35}$$

This leads us to

$$\frac{\rm i}{\hbar}\langle[\hat{\mathcal{H}}_{\rm int},\hat{\mathcal{H}}_{\rm cm}]\rangle = \frac{{\rm i}\hbar\omega}{2}\Bigg\langle\sum_{m,n}(n-m)|m\rangle \times\langle n|\Big[\big(g_1^*|1\rangle\langle 3| + g_2|3\rangle\langle 2|\big)F^{(-\eta)}_{mn} + (g_1|3\rangle\langle 1| + g_2^*|2\rangle\langle 3|)F^{(+\eta)}_{mn}\Big]\Bigg\rangle. \tag{36}$$

We may separate this expression into

$$\langle\dot{\mathcal{E}}^1_{\rm int}\rangle = \frac{\rm i}{2}\sum_{n,p}(n-p)\left[g_1^*\rho_{3n1p}F^{(-\eta)}_{pn} + g_1\rho_{1n3p}F^{(+\eta)}_{pn}\right], \tag{37}$$

$$\langle\dot{\mathcal{E}}^2_{\rm int}\rangle = \frac{\rm i}{2}\sum_{n,p}(n-p)\left[g_2\rho_{2n3p}F^{(-\eta)}_{pn} + g_2^*\rho_{3n2p}F^{(+\eta)}_{pn}\right], \tag{38}$$

where $\langle\dot{\mathcal{E}}_{\rm int}\rangle = \langle\dot{\mathcal{E}}^1_{\rm int}\rangle + \langle\dot{\mathcal{E}}^2_{\rm int}\rangle$. Equations (37) and (38) can be explained as follows. In absorption and stimulated emission processes from each laser, there is a possibility of changing the vibrational level. The probability of change is dictated by the Franck-Condon factor. The sign convention used for the weight of the respective energy change, $(n-p)\hbar\omega$, is that of Eq. (30). It implies that a negative value of $\langle\dot{\mathcal{E}}_{\rm int}\rangle$ describes loss of vibrational energy from the trapped atom.

As is apparent from Fig. (3), these vibrationally off-diagonal transitions occur in the vicinity of the EIT resonance position with greatly different strength in heating ($\delta_{\rm eff} < 0$) and cooling events ($\delta_{\rm eff} > 0$). Under the condition $\Delta_1 = \Delta_2 = \Delta$, the sum of Eqs. (37) and (38) equates to an overall negative value when $\Delta > 0$, whereas it is positive (that is, heating) for $\Delta < 0$. In our simulation, we find that the integrated energy loss,

$$\langle\mathcal{E}_{\rm int}(t)\rangle = \int_0^t dt'\langle\dot{\mathcal{E}}_{\rm int}(t')\rangle, \tag{39}$$

exceeds the total vibrational energy loss by a small amount. This excess of cooling is just balanced by the vibrational heating incurred in spontaneous emission, the second term in Eq. (34). As we show in the appendix VI, the rate of vibrational energy transfer in spontaneous emission is

$$\langle\mathcal{E}_{\rm sp}\rangle = \sum_j \Gamma_j\eta^2{\rm tr}\{|3\rangle\langle 3|\hat{\tilde{\rho}}\} = \Gamma\eta^2\sum_n\tilde{\rho}_{3n3n}, \tag{40}$$

where we have used $\Gamma_1 = \Gamma_2 = \Gamma/2$. The quantity in Eq. (40) is always positive and expresses the fact that in spontaneous emission, the summed strength of sidebands with $m > n$ always exceeds that of the sidebands with $m < n$, thus effectively heating the vibrational degree of freedom.[4] The energy loss rates from Eq. (34) are shown in Figs. 6(a) and 6(b). Their sum, added to the initial vibrational energy, is compared to the time development of $\langle n\rangle$ in Fig. 6(c). We see that the rate of heating by spontaneous emission is smaller than the rate of cooling due to interaction with the two lasers by a factor of about sixty. We find numerically

$$\langle n(t)\rangle = n_{\rm init} + \int_0^t dt'(\langle\dot{\mathcal{E}}_{\rm int}(t')\rangle + \langle\dot{\mathcal{E}}_{\rm sp}(t')\rangle) \tag{41}$$

and conclude that the two terms in Eq. (34) correctly reproduce the rate of cooling. Hence, they should also contain the explanation on where the vibrational energy is transferred. It turns out that for the trapped atom, the sole mechanism for cooling relies on inelastic scattering of laser radiation by the trapped atom. To prove this point, we examine in the following section the radiation fields emitted by the trapped atom.

IV. RADIATION FIELD SCATTERED BY THE TRAPPED ATOM

In order to study the temporal development of the scattered radiation spectrum during the process of cooling, we consider the two-time correlation function

$$\mathcal{S}^q_j(t,\tau) = \langle\sigma^+_{jq}(t)\sigma^-_{jq}(t-\tau)\rangle. \tag{42}$$

Here t signifies some arbitrary point in time during the cooling process at which a photon is scattered.

A. Steady-state spectrum

In steady state, the two-time correlation function is independent of t, and we obtain the spectral distribution of scattered radiation per frequency interval by Fourier transformation of Eq. (42),

$$\mathcal{S}^q_j(\omega') = {\rm Re\ tr}\{\sigma^+_{jq}({\rm i}\omega' - \hat{\mathcal{L}})^{-1}\sigma^-_{jq}\hat{\tilde{\rho}}_{\rm st}\}, \tag{43}$$

where $\tilde{\rho}_{\rm st}$ is the stationary-state density operator, and $\hat{\mathcal{L}}$ represents the Lindblad generator of the master equation (4). Note that ω' refers to different absolute frequency scales for each laser. The spectrum contains inelastic Mollow and Raman contributions in a narrow frequency band around the laser frequency ω_{L_j}. We have defined $\omega' = \omega_k - \omega_{L_j}$, where ω_k refers to the scattered radiation frequency. Numerical results for the steady-state spectra, ($\mathcal{S}_j = \mathcal{S}^{+1}_j + \mathcal{S}^{-1}_j$), obtained from Eq. (43) are shown in Fig. 7. The spectra are centered around the two laser frequencies, ω_{L_1} and ω_{L_2}. Both spectra show the elastic Rayleigh peak at $\omega' = 0$. This peak does not contribute to an internal energy change of the trapped atom. However, the different strengths of red and blue sidebands in each

[4]This statement is true when the harmonic oscillators that describe the trapping of ground and excited states of the atom coincide spatially. This need not be true in the case where the HO states of ground and excited states are spatially separated.

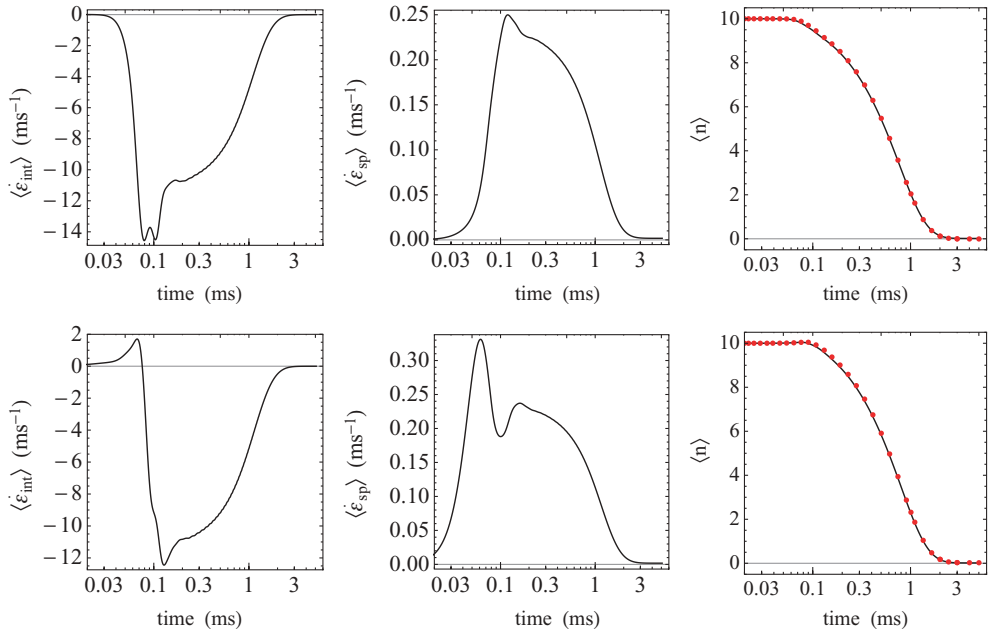

FIG. 6. (Color online) Vibrational energy transfer rates from Eq. (34) are shown in the left and center images. The time-integrated loss rate is compared to the value of $\langle n \rangle$ in the right images Eq. (41). The top row gives the result when the initial Fock state ($n = 10$) is in the electronic state $|2\rangle$. In the bottom row, the system is initially in the electronic state $|1\rangle$.

spectrum points to fluctuating changes in the internal energy of the trapped atom. We note that the radiation scattered in the strong laser transition emphasizes red sidebands over blue sidebands. The reverse is true for the weak laser. One might say that in steady-state the trapped atom (which has nearly reached EIT conditions) preferentially scatters photons from laser 2 into red sidebands of laser 1 and photons from laser 1 into blue sidebands of laser 2. Blue sidebands in the spectrum emitted by the interaction with laser 2 refer to scattering transitions $|3n\rangle \rightarrow |2m\rangle$ with $m < n$. On the other hand, red sidebands in the spectrum emitted by the interaction with laser 1 refer to scattering transitions $|3n\rangle \rightarrow |1m\rangle$ with $m > n$, thus balancing cooling and heating in steady state. The spectral features in Fig. 7 are not Mollow-type sidebands; rather, they should be classified as nonlinear Raman scattering. The actual Mollow sidebands lie outside the frequency range shown in Fig. 7. The reason for this is the large detuning chosen in our example, $\Delta = 2\pi \times 15$ MHz. The Mollow sidebands are visible on the double logarithmic scale in Fig. 8.

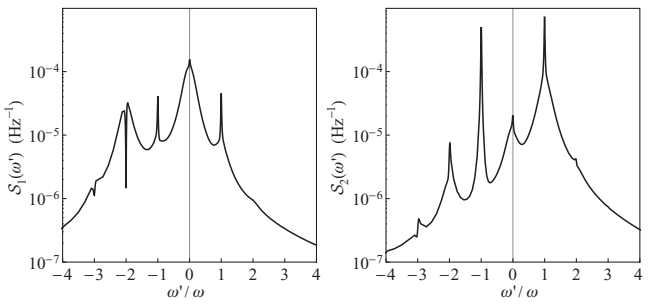

FIG. 7. Steady-state spectral distribution of scattered radiation from the strong laser 1 (left) and from laser 2 (right) in the immediate vicinity of the elastic peaks.

Here, both blue and red sidebands are shown on a common, absolute frequency axis. Under stationary-state conditions, the energetic balance of the summed contributions from scattering events terminating in the two ground states should be zero, as in our steady-state calculation the small amount of heating from $\langle \dot{\mathcal{E}}_{\rm int} \rangle^{\rm st}$ very precisely balances the spontaneous heating term $\langle \dot{\mathcal{E}}_{\rm sp} \rangle^{\rm st}$. We note here that the steady-state resonance fluorescence generated by one of the lasers has been studied analytically in the Lamb-Dicke limit by Bienert*et al.* [12]. Our numerical predictions agree with their results if we restrict the allowed sidebands to $\Delta n = \pm 1$.

The origin of the Mollow sidebands and their frequency position in relation to the Raman sidebands can be understood with the help of Fig. 9, which uses the dressed-state labels $|i, n, N\rangle = |$electronic, vibrational, photon state$\rangle$ (N referring to the photons of the strong laser 1) in the left-hand part of the figure. The Mollow peaks in Fig. 8(a) result from

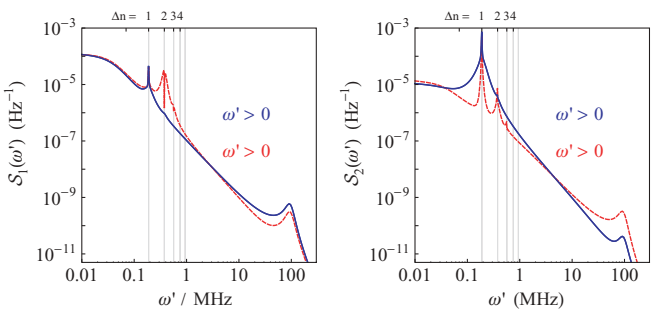

FIG. 8. (Color online) Steady-state spectral distribution of scattered radiation from the strong laser 1 (left) and from laser 2 (right) including the Mollow contributions. The spectral contributions at frequencies $\omega' < 0$ are given by the dashed lines; the full lines refer to $\omega' > 0$.

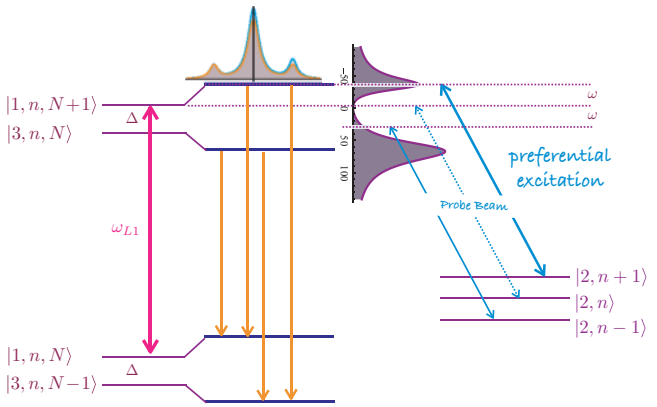

FIG. 9. (Color online) Excitation profile and Mollow triplet under EIT conditions with blue detuning. In our example, the actual ratio of $\omega : \Delta = 1 : 500$.

transitions from the manifold $|3,n,N\rangle, |1,n,N+1\rangle$ to the manifold $|3,n,N-1\rangle, |1,n,N\rangle$ at separations $\pm\Delta$ from the elastic peak. The left part of Fig. 9 depicts the absorption profile from different vibrational levels n, experienced by laser 2. Note that in order to achieve EIT cooling, we have chosen the ac-Stark shift to be of similar magnitude to the vibrational trap frequency, ω. In our numerical example, the latter is a factor of 500 smaller than the detuning Δ. As a consequence, the Raman sidebands concentrate into a narrow range around the elastic peak; see Figs. 7 and 8. If we consider the action of a strong pump laser in the 1–3 transition at a specific vibrational level, n, a balanced Mollow triplet should appear centered at the laser frequency ω_{L1}. The laser acting on the 2–3 transition at the same vibrational level n fulfills EIT conditions and does not disturb this situation. However, this laser can act from the adjacent vibrational levels $n \pm 1$. At blue detuning, it will preferentially pump from $n+1$. This preferentially feeds the blue sideband of the Mollow triplet, thereby transferring vibrational energy into the scattered radiation field.

B. Time dependence of scattered radiation

In the time-dependent case, we are required to resort to an explicit calculation of the two-time-correlation function for each laser. The quantum regression originally proposed by Lax [13] allows us to calculate multitime correlation functions from the knowledge of single-time expectation values, which in turn implies the knowledge of the density matrix evolution [10,14–16],

$$\langle\sigma_{jq}^{+}(t)\sigma_{jq}^{-}(t-\tau)\rangle = \mathrm{tr}\{\sigma_{jq}^{+}e^{\mathcal{L}\tau}\sigma_{jq}^{-}e^{\mathcal{L}(t-\tau)}\hat{\rho}(t=0)\}. \quad (44)$$

For the calculation, we are required to choose the scattering angle θ as it controls the magnitude of η via the exponential terms in the Lindblad operators (12). We have carried out this calculation for scattering from each laser in the direction parallel and antiparallel to the trap axis.[5] The frequency spectrum of scattered radiation at any time t is finally obtained by Fourier transformation of the two-time-correlation

[5]The angular spectra show a pronounced dependence on θ, with vibrational sidebands being absent for $\theta = \pi/2$.

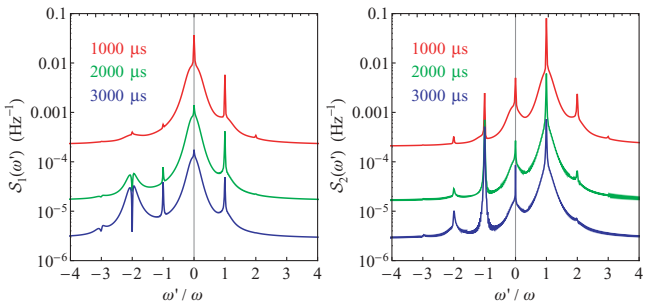

FIG. 10. (Color online) Temporal development of radiation scattered from each laser beam during the cooling process. The result for the strong laser 1 is given in the left figure, and that of laser 2 is given in the right figure. The spectra are calculated at the times indicated in each figure.

function,

$$\mathcal{S}_j^q(\omega',t) = \mathrm{Re}\int_0^t d\tau\,\langle\sigma_{jq}^{+}(t)\sigma_{jq}^{-}(t-\tau)\rangle e^{-i\omega_j'\tau}. \quad (45)$$

Examples of the temporal development of radiation scattered from each laser beam during the cooling process are given in Fig. 10. It is apparent that during the cooling process blue sidebands prevail for both transitions, contrary to the steady-state situation discussed previously. As cooling proceeds, the prevalence of the blue sidebands decreases until the steady-state situation seen in Fig. 7 is reached. This reduction in the cooling rate by preferential emission of blue sidebands is more clearly seen in Fig. 11, which gives the sum of the spectra from both lasers as a function of time t, as well as, for comparison, the steady-state result calculated from Eq. (43).

C. Energy removal by scattered radiation

To pinpoint the essential mechanism for EIT cooling of a trapped atom, we explore in a quantitative manner the energy

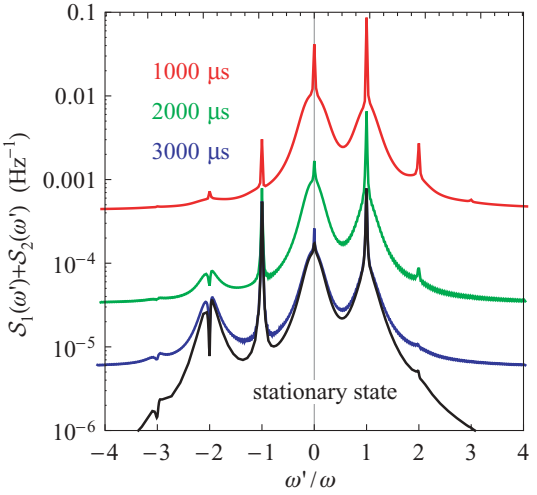

FIG. 11. (Color online) Summed spectra of scattered radiation show preferential blue emission at early times in the cooling process. As the cooling proceeds, the stationary-state spectrum predicted from Eq. (43) is reached. The spectra are calculated at the times indicated in the figure.

removed from the atom by the scattered radiation. We show here that the vibrational energy loss rate in cooling, Eq. (34) and Fig. 6, can be found in the form of blue sidebands in the spectrum of scattered radiation, a context testifying to the consistency of our numerical approach. We find that in the course of cooling, the imbalance in the sidebands diminishes, precisely as predicted by the rate of energy removal; see Eq. (41).

The energy dissipated by a trapped atom due to inelastic scattering of laser radiation out of the incident laser fields as resonance fluorescence can be explored by calculating the time evolution of scattered quanta. The imbalance of the total power delivered to the quantized radiation field is given by Eq. (27), which we repeat here for convenience:

$$\mathcal{R}(t) = \sum_j \frac{\hbar\Gamma_j}{2\pi} \int_{-\infty}^{+\infty} d\omega'\omega' \big[\mathcal{S}_j^{+1}(\omega', t) + \mathcal{S}_j^{-1}(\omega', t)\big]. \quad (46)$$

The frequency integrals in this equation can be expressed by

$$\int_{-\infty}^{+\infty} d\omega'\omega' \mathcal{S}_j^q(\omega', t) = -\pi \mathrm{Re}\left[\mathrm{i}\frac{d}{d\tau}\langle\sigma_{jq}^+(t)\sigma_{jq}^-(t-\tau)\rangle\right]_{\tau=0}, \quad (47)$$

which, in turn, can be written with the help of the master equation (4) as

$$\int_{-\infty}^{+\infty} d\omega'\omega' \mathcal{S}_j^q(\omega', t) = -\frac{\pi}{\hbar}\mathrm{Re}\langle\sigma_{jq}^+[\hat{\mathcal{H}}, \sigma_{jq}^-]\rangle. \quad (48)$$

Thus, we find

$$\mathcal{R}(t) = -\sum_{j,q} \frac{\Gamma_j}{2}\mathrm{Re}\langle\sigma_{jq}^+[\hat{\mathcal{H}}, \sigma_{jq}^-]\rangle. \quad (49)$$

On the other hand, the master equation leads to the following expression for the total energy loss of the system:

$$\frac{d}{dt}\langle\hat{\mathcal{H}}\rangle = \langle\hat{\mathcal{L}}_0^\dagger\hat{\mathcal{H}}\rangle = \sum_{j,q}\frac{\Gamma_j}{2}\mathrm{Re}\langle\sigma_{jq}^+[\hat{\mathcal{H}}, \sigma_{jq}^-]\rangle, \quad (50)$$

where $\hat{\mathcal{L}}_0^\dagger$ denotes the adjoint Lindblad generator [10]. Hence, we see that

$$\mathcal{R}(t) = -\frac{d}{dt}\langle\hat{\mathcal{H}}\rangle. \quad (51)$$

This equation shows that the imbalance of the total energy transferred per unit of time to the quantized radiation field is equal to the negative rate of change of the total energy of the system, thus confirming our definition of $\mathcal{R}(t)$ in Sec. II B. Equation (51) may be written as

$$\mathcal{R}(t) + \frac{d}{dt}\langle\hat{\mathcal{H}}_{\mathrm{cm}}\rangle = -\frac{d}{dt}\langle\hat{\mathcal{H}}_{\mathrm{el}} + \hat{\mathcal{H}}_{\mathrm{int}}\rangle = -\langle\mathcal{L}_0^\dagger(\hat{\mathcal{H}}_{\mathrm{el}} + \hat{\mathcal{H}}_{\mathrm{int}})\rangle + \frac{\mathrm{i}}{\hbar}\langle[\hat{\mathcal{H}}_{\mathrm{int}}, \hat{\mathcal{H}}_{\mathrm{cm}}]\rangle. \quad (52)$$

The expression on the left-hand side of this equation enables a direct comparison of the excess power gained by the scattered radiation field, $\mathcal{R}(t)$, and the vibrational cooling rate of the atom, $\frac{d}{dt}\langle\hat{\mathcal{H}}_{\mathrm{cm}}\rangle$. In Fig. 12, we compare $\mathcal{R}(t)$ with the negative cooling rate $-d\langle\hat{\mathcal{H}}_{\mathrm{cm}}\rangle/dt$ given in Eq. (34). We see that the power loss due to unbalanced scattering of radiation nearly matches the negative cooling rate. This proves that in EIT cooling, the vibrational energy is removed from the trapped atom in the form of of scattered radiation with unbalanced vibrational sidebands. We observe, however, a small difference between $\mathcal{R}(t)$ and $-d\langle\hat{\mathcal{H}}_{\mathrm{cm}}\rangle/dt$. This difference is explained by the right-hand side of Eq. (52). During the exponential cooling period ($t > 100\ \mu$s), this difference amounts to about 10% of the spectral imbalance in the example shown here. Thus, we see that during the exponential cooling phase 90% of the unbalanced radiative energy loss, $\mathcal{R}(t)$, leads to vibrational cooling of the HO, while the remaining 10% contributes to the loss of the energy of the internal degree of freedom, $-\frac{d}{dt}\langle\hat{\mathcal{H}}_{\mathrm{el}}\rangle$, and to the loss of the interaction energy between the atom and the external laser fields, $-\frac{d}{dt}\langle\hat{\mathcal{H}}_{\mathrm{int}}\rangle$. The exponential decrease of the latter two quantities is a manifestation of the fact that the atom approaches near-EIT (dark-state) conditions, thus decoupling from the driving laser fields.

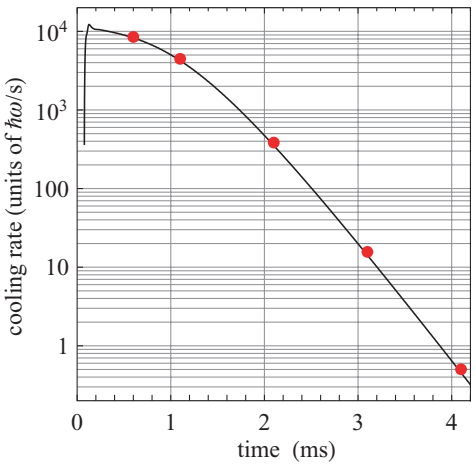

FIG. 12. (Color online) Cooling rate $\mathcal{R}(t)$ resulting from unbalanced scattering of laser radiation from Eq. (46) is given by the dots. It closely follows the predictions for the negative cooling rate $-d\langle\hat{\mathcal{H}}_{\mathrm{cm}}\rangle/dt$ obtained by adding Eqs. (37), (38), and (40), which is represented by the full line.

V. OBSERVATIONS AND DISCUSSION

We have studied numerous examples like the ones discussed in the previous sections in order to investigate realistic laboratory parameters appropriate for cooling trapped neutral atoms using the EIT concept. From these studies, we derive the following general statements on the time-dependent and stationary-state solutions of the master equation (4).

The concept of EIT cooling appears feasible for neutral atoms, even at elevated values of the Lamb-Dicke parameter, at least as long as the Lamb-Dicke parameter stays less than ≈ 0.5. Note that $\eta \approx 1$ is equivalent to losing vibrational selectivity, hence negating the very basic concept of vibrational cooling.

Blue detuning, that is, $\Delta_1 = \Delta_2 > 0$, and two-photon resonance of the interacting lasers is tantamount for success of the EIT-cooling concept. The two-photon resonance condition is likely the most stringent experimental requirement when cooling neutral atoms. As neutral-atom-trap frequencies are typically small (usually less than 100 kHz), the two-photon

resonance condition can only be met when the frequencies of the lasers are significantly less than the trap frequency. At the same time, external-field-induced energy shifts of the electronic ground-state levels must be kept spatially constant over the cooling region at a level *well less than* the trap frequency. Provided that these conditions can be met, the EIT-cooling concept works regardless of the magnitude of g_1 and g_2. This is equivalent of saying that high power stability of the lasers is not a prerequisite of this cooling concept. It is also only weakly dependent on the absolute amount of blue detuning.

Unequal values of g_1 and g_2 makes EIT cooling more effective with regard to the cooling limit, $\langle n\rangle_{\rm lim}$, which decreases when one of the Rabi rates is made very small. This benefit goes at the cost of increased time required for cooling. Cooling occurs even at equal laser intensities, but $\langle n\rangle_{\rm lim}$ is slightly greater then. A further general result is that a decrease of the excited-state radiative rate, Γ, leads to reduction of $\langle n\rangle_{\rm lim}$ and the cooling rate. Not unexpectedly, we find that for red-detuned laser beams, $\Delta_1 = \Delta_2 < 0$, a rapid vibrational heating occurs.

At very low values of η, cooling is optimal if one of the lasers causes an ac-Stark shift about equal to the trap vibrational energy, the basic concept that led Morigi *et al.* [2] to introduce this concept in the first place. We find that for higher values of η, cooling can be optimized by covering several sidebands in the ac-Stark shift resonance wing. For example, this feature is borne out by the appearance of a second minimum in Fig. 6 of Ref. [6]. The rate of cooling, of course, increases with increasing Lamb-Dicke parameter, as has been pointed out previously [5]. At long cooling times and in the stationary-state solution, the population ratio in the electronic ground states is found to be $\sum_n \rho_{1n1n}/\sum_n \rho_{2n2n} \approx (g_2/g_1)^2$, a result that is exact for EIT in a free atom with copropagating beams or the trapped atom in the Lamb-Dicke limit ($\eta \to 0$). The numerical cooling results are identical regardless of whether we initially start from a Fock state in electronic state $|1\rangle$ or $|2\rangle$. The congruence of numerical results obtained by analyzing the trapped-atom energy loss and the power emerging in the scattered radiation field, and the numerical agreement between the left- and right-hand sides of Eqs. (28), (41), and (51), testify to the reliability of the numerical approach we use.

VI. CONCLUSION

The numerical solution of the dynamics of a three-level atom trapped in a harmonic potential has given us new insights into the physics of vibrational cooling by EIT. Our numerical approach allows the simulation of the full quantum master equation for this situation far from the Lamb-Dicke limit and thus enables us to trace realistic histories of a trapped atom in its approach to the nonequilibrium stationary state. The latter is represented by the near-dark state of the atom in the presence of the two laser fields that drive EIT. Obviously, all energy lost from the atomic system is ultimately transferred to the reservoir of quantized radiation modes during the cooling process. In the present example, the spectrum of photons emitted into this reservoir carries the signatures of nonlinear Raman scattering of the two laser beams by the trapped atom. These features of the scattered radiation spectrum are responsible for the rapid removal of trap vibrational energy and hence atomic cooling.

As we have demonstrated, the numerical approach permits a quantitative comparison between the energy imbalances in the time-dependent spectra of scattered radiation and the dissipation of the energy of the atom-laser system. It further allows separation of the individual contributions to the total energy loss provided by the change of the harmonic oscillator energy, the internal electronic energy, and the atom-laser interaction energy. This explicit separation of the individual decay channels opens a door to an intimate examination of the underlying dynamics.

The time-dependence of laser radiation scattered by the trapped atom demonstrates the precise rate of vibrational cooling. The temporal sequence of events during the cooling cycle is most interesting and educational. In every case, we find that after an initial period of *equilibration*, during which the trapped atom first responds to the turn-on of the external laser fields and finally reaches a kind of quasistationary state with a slow time dependence on the relevant variables, the mean values of the atomic momentum and position are damped exponentially. This dynamics is critically controlled by the atomic susceptibilities. The latter emphasize blue sideband scattering during the cooling process, the preferred path of energy removal from the trapped atom. Also in the stationary state, the spectrum of scattered radiation carries signatures of the dynamics of energy redistribution. This is required because the small leakage of spontaneous photons in the near-dark state has to be compensated by vibrational cooling transitions. The system achieves this balance by a redistribution of sidebands between the two counterpropagating laser beams.

Finally, we also observed the emergence of strong quantum correlations and entanglement between the external translational and the internal electronic degrees of freedom of the trapped atom during the cooling process. In particular, we found that the final state reached for long cooling times represents a nonequilibrium stationary state, which exhibits clear signatures of mixed-state entanglement. The time evolution of entanglement and its corresponding stationary-state value are the most intriguing features that accompany the dynamics of cooling. These topics will be discussed in a forthcoming article.

ACKNOWLEDGMENTS

This research was supported by the Deutsche Forschungsgemeinschaft, Grant HE-2525/8.

APPENDIX: SPONTANEOUS HEATING RATE

The rate of energy transfer in spontaneous emission, which appears as the second part of Eq. (34), is given by

$$\begin{aligned}\langle \mathcal{E}_{\rm sp}\rangle &= \mathrm{tr}\left[\left(\frac{\hat{\mathcal{P}}^2}{2}+\frac{\hat{\mathcal{Q}}^2}{2}\right)\hat{\mathcal{L}}_0\hat{\tilde{\rho}}\right]\\ &= \sum_{jq}\frac{\Gamma_j}{2}\mathrm{tr}\left\{\left(\frac{\hat{\mathcal{P}}^2}{2}+\frac{\hat{\mathcal{Q}}^2}{2}\right)\left[\sigma_{jq}^-\hat{\tilde{\rho}}\sigma_{jq}^+-\frac{1}{2}\left\{\sigma_{jq}^+\sigma_{jq}^-,\hat{\tilde{\rho}}\right\}\right]\right\}.\\ &= \sum_j\Gamma_j\mathrm{tr}\left\{\left[\mathrm{e}^{-\mathrm{i}\sqrt{2}\eta\mathcal{Q}}\left(\frac{\hat{\mathcal{P}}^2}{2}+\frac{\hat{\mathcal{Q}}^2}{2}\right)\mathrm{e}^{\mathrm{i}\sqrt{2}\eta\mathcal{Q}}\right.\right.\\ &\quad\left.\left.-\left(\frac{\hat{\mathcal{P}}^2}{2}+\frac{\hat{\mathcal{Q}}^2}{2}\right)\right]|3\rangle\langle 3|\hat{\tilde{\rho}}\right\}. \qquad \text{(A1)}\end{aligned}$$

By rewriting

$$\left[\mathrm{e}^{-\mathrm{i}\sqrt{2}\eta\mathcal{Q}}\left(\frac{\hat{\mathcal{P}}^2}{2}+\frac{\hat{\mathcal{Q}}^2}{2}\right)\mathrm{e}^{\mathrm{i}\sqrt{2}\eta\mathcal{Q}}-\left(\frac{\hat{\mathcal{P}}^2}{2}+\frac{\hat{\mathcal{Q}}^2}{2}\right)\right] = \mathrm{e}^{-\mathrm{i}\sqrt{2}\eta\mathcal{Q}}\left[\left(\frac{\hat{\mathcal{P}}^2}{2}+\frac{\hat{\mathcal{Q}}^2}{2}\right)\mathrm{e}^{\mathrm{i}\sqrt{2}\eta\mathcal{Q}}\right] \tag{A2}$$

and applying the momentum operator, $\hat{\mathcal{P}}=-\mathrm{i}(\partial/\partial\mathcal{Q})$, we obtain for the rate of vibrational energy transfer in spontaneous emission

$$\langle\dot{\mathcal{E}}_{\mathrm{sp}}\rangle=\sum_j\Gamma_j\eta^2\mathrm{tr}\{|3\rangle\langle 3|\rho\}=\Gamma\eta^2\sum_n\tilde{\rho}_{3n3n}, \tag{A3}$$

where we have used $\Gamma_1=\Gamma_2=\Gamma/2$.

[1] M. Lindberg and J. Javainen, J. Opt. Soc. Am. B **3**, 1008 (1986).

[2] G. Morigi, J. Eschner, and C. H. Keitel, Phys. Rev. Lett. **85**, 4458 (2000).

[3] F. Schmidt-Kaler, J. Eschner, G. Morigi, C. F. Roos, D. Leibried, A. Mundt, and R. Blatt, Appl. Phys. B **73**, 807 (2001).

[4] J. Lawall, S. Kulin, B. Saubamea, N. Bigelow, M. Leduc, and C. Cohen-Tannoudji, Phys. Rev. Lett. **75**, 4194 (1995).

[5] G. Morigi, Phys. Rev. A **67**, 033402 (2003).

[6] M. Roghani and H. Helm, Phys. Rev. A **77**, 043418 (2008).

[7] B. Karl, *Density Matrix Theory and Applications* (Plenum Press, New York, 1981).

[8] M. Orszag, *Quantum Optics* (Springer, Berlin, 2000).

[9] P. Meystre, *Atom Optics* (Springer, New York, 2001).

[10] H. P. Breuer and F. Petruccione, *The Theory of Open Quantum Systems* (Oxford University Press, Oxford, 2007).

[11] C. W. Gardiner and P. Zoller, *Quantum Noise: A Handbook of Markovian and Non-Markovian Quantum Stochastic Methods with Applications to Quantum Optics* (Springer, Berlin, 2004), p. 377.

[12] M. Bienert, W. Merkel, and G. Morigi, Phys. Rev. A **69**, 013405 (2004).

[13] M. Lax, Phys. Rev. **129**, 2342 (1963); **157**, 213 (1967).

[14] M. O. Scully and M. S. Zubairy, *Quantum Optics* (Cambridge University Press, Cambridge, 1997).

[15] P. Meystre, and M. Sargent III, *Elements of Quantum Optics* (Springer, Berlin, 2007), p. 376.

[16] H. J. Carmichael, *An Open Systems Approach to Quantum Optics* (Springer, Berlin, 1993).